

ON THE ANALYTICAL SOLUTIONS AND NUMERICAL VERIFICATIONS OF THE TWO-PHASE WATER FAUCET PROBLEM

Ling Zou^{*}, Haihua Zhao, and Hongbin Zhang

Idaho National Laboratory

P.O. Box 1625, Idaho Falls, ID 83415-3870 USA

ling.zou@inl.gov; haihua.zhao@inl.gov; hongbin.zhang@inl.gov

ABSTRACT

The one-dimensional water faucet problem is one of the benchmark problems originally proposed by Ransom for two-phase flow studies. The test problem consists of a vertical pipe, which is initially filled with a uniform column of liquid moving with a prescribed initial velocity and an annulus of gas sitting still. At the top boundary, liquid is supplied at the same velocity as the initial velocity, and the bottom of the pipe opens to the ambient. Due to the gravity effect, the liquid column accelerates and becomes thinner as it descends. With certain simplifications, such as massless gas phase and no wall and interfacial frictions, analytical solutions had been previously obtained for the transient liquid velocity and void fraction distribution. This test problem and its analytical solutions have been widely used for the purposes of code assessment, benchmark and numerical verifications. In our previous study, it was used for the mesh convergence study of a high-resolution spatial discretization scheme. It was found that, at the steady state, an expected second-order spatial accuracy could not be achieved when compared to the existing analytical solutions. A further investigation showed that the existing analytical solutions do not actually satisfy the commonly used two-fluid single-pressure two-phase flow equations. In this work, we will demonstrate the derivation of an extension of Ransom's transient solutions with the assumption of separate water and gas pressures and a new set of analytical solutions for the steady-state conditions with the single pressure assumption. The transient analytical solutions are compared to the numerical results with a first-order and a high-resolution spatial discretization schemes. The steady state analytical solutions are used for mesh convergence studies, from which expected second-order of accuracy is achieved for the 2nd order scheme.

KEYWORDS

Two-phase flow, water faucet problem, analytical solutions, numerical verification

1. INTRODUCTION

The water faucet problem is one of the two-phase flow benchmark problems originally proposed by Ransom [1]. This test problem and its analytical solutions have been widely used for the purposes of code assessment, benchmark and numerical verification. This problem was originally proposed to test the interaction of the body force terms with the acceleration term in the momentum equations of the two-phase flow models. With certain simplifications, such as massless gas phase, no wall and interfacial frictions, and no pressure variations in the liquid phase, analytical solutions have been previously obtained for the transient liquid phase velocity and void fraction distribution by Ransom [2]. This problem has been selected for the purpose of reactor safety analysis code assessment, such as RELAP5-3D [2] and MARS [3]. It has also been widely used in the studies on new numerical algorithms [4-9], on new two-phase models [10-12], and on the study of the non-hyperbolic nature of the single-pressure two-phase two-fluid models [13]. In most of these existing studies, the analytical solutions proposed by Ransom were used as references for the purpose of comparisons with the numerical results. Only a few of

those studies [4-5, 9, 11-12] performed mesh convergence studies using the Ransom's solutions as references. All of these convergence studies were performed in transient situations, in which discontinuities are still present in the void fraction distribution. As expected, the expected order of accuracy cannot be obtained due to the discontinuities in the solutions (see section 8.7 of [14] for more details).

In our previous work [15], the Ransom's solutions were used for the convergence study of a high-resolution spatial discretization scheme using staggered grids. The high-resolution spatial discretization scheme has a second-order spatial accuracy for solutions in smooth regions. However, when using the Ransom's solution as the reference, it was found that a second-order of accuracy could not be obtained, even at the steady state at which all solutions are smooth in space. By carefully examining the water faucet problem and the single-pressure two-phase flow model, we concluded that new analytical solutions could be derived under steady-state condition. In this paper, an extension of the Ransom's solutions to include the transient distributions of gas phase velocity and pressure will be presented first. The derivation of the new analytical solutions for the steady-state conditions will ensue for the water faucet problem. Numerical verification using a first-order and a high-resolution spatial discretization schemes will be presented for comparison with both the transient and the steady-state analytical solutions.

2. TWO-PHASE FLOW MODEL AND WATER FAUCET PROBLEM

2.1. Simplified Two-phase Flow Model

For the two-phase flow model, we are particularly interested in the single-pressure, two-fluid, two-phase flow equations, which are commonly used in the existing system analysis codes, such as RELAP5 [17], TRAC [18], and TRACE [19]. The water faucet problem is a hydrodynamics problem, in which the internal energies of both phases do not change. Thus, in this study, the energy equations of both phases are omitted. The water faucet problem also assumes no wall friction and no interfacial friction between the two phases. Based on these simplifications and assumptions, a four-equation set for the two-phase flow could be obtained,

$$\frac{\partial(\alpha_l \rho_l)}{\partial t} + \frac{\partial(\alpha_l \rho_l u_l)}{\partial x} = 0 \quad (1)$$

$$\frac{\partial(\alpha_g \rho_g)}{\partial t} + \frac{\partial(\alpha_g \rho_g u_g)}{\partial x} = 0 \quad (2)$$

$$\frac{\partial u_l}{\partial t} + u_l \frac{\partial u_l}{\partial x} + \frac{1}{\rho_l} \frac{\partial p}{\partial x} - g = 0 \quad (3)$$

$$\frac{\partial u_g}{\partial t} + u_g \frac{\partial u_g}{\partial x} + \frac{1}{\rho_g} \frac{\partial p}{\partial x} - g = 0 \quad (4)$$

in which the subscripts l and g denote the liquid phase and the gas phase, respectively. The variables to be solved from this set of equations are p , α_g , u_l , and u_g , which are pressure, void fraction (volume fraction of the gas phase), liquid phase velocity, and gas phase velocity, respectively. Note that $\alpha_l = 1 - \alpha_g$. This set of equations is closed by equations of state for both phases. For simplicity, linearized barotropic equations of state are used in this study for both phases:

$$\begin{aligned}\rho_l(p) &= \rho_{l,0} + \frac{1}{\left(\frac{dp}{d\rho_l}\right)_0} (p - p_0) \\ \rho_g(p) &= \rho_{g,0} + \frac{1}{\left(\frac{dp}{d\rho_g}\right)_0} (p - p_0)\end{aligned}\tag{5}$$

in which, $\rho_{l,0} = 10^3 \text{ kg/m}^3$, $\rho_{g,0} = 0.5 \text{ kg/m}^3$, and $p_0 = 10^5 \text{ Pa}$, are reference liquid phase density, reference gas phase density, and reference pressure, respectively. $\left(\frac{dp}{d\rho_l}\right)_0 = 10^7 \text{ Pa/(kg/m}^3)$ and $\left(\frac{dp}{d\rho_g}\right)_0 = 10^6 \text{ Pa/(kg/m}^3)$ reflect the compressibility of the liquid phase and gas phase, respectively. It is noted that the choice of equation of state will not affect the mathematical derivations in the following work.

2.2. Water Faucet Problem Description

The one-dimensional water faucet problem consists of a vertical pipe of length L . Initially, the pipe is filled with a uniform column of liquid moving with velocity $u_{l,init}$ and an annulus of gas moving with velocity $u_{g,init}$. The initial void fraction (gas phase volume fraction) is $\alpha_{g,init}$, and the initial pressure is p_{init} . Due to the gravity effect, the liquid column accelerates and becomes thinner with time. A schematic drawing of the water faucet problem is shown in **Figure 1**. The initial and boundary conditions for the water faucet problem are summarized in **Table I**. With certain simplifications such as massless gas phase, no wall and interfacial frictions, and no pressure variations in the liquid phase, analytical solutions had been previously obtained for the transient liquid velocity and void fraction distribution [20] (hereafter referred to as the Ransom's solutions). Some details of the derivation can also be found in [6, 21]. A derivation for the steady-state conditions can be found in [2].

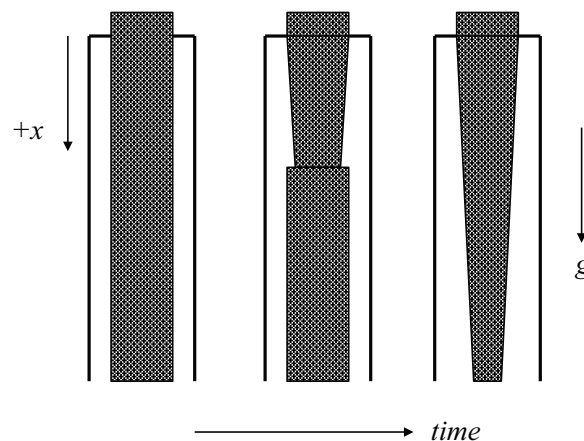


Figure 1. Schematic drawing of the two-phase water faucet problem.

The Ransom's solutions provide the transient distributions of liquid velocity and void fraction along the pipe length:

$$u_l(x, t) = \begin{cases} \sqrt{u_{l,init}^2 + 2gx} & \text{if } x \leq u_{l,init}t + gt^2/2 \\ u_{l,init} + gt & \text{otherwise} \end{cases}\tag{6}$$

and,

$$\alpha_g(x, t) = \begin{cases} 1 - \frac{(1 - \alpha_{g,init})u_{l,init}}{\sqrt{u_{l,init}^2 + 2gx}} & \text{if } x \leq u_{l,init}t + gt^2/2 \\ \alpha_{g,init} & \text{otherwise} \end{cases} \quad (7)$$

Under the steady-state conditions, the Ransom's solutions (Equations (6) and (7)) simply become,

$$u_{l,ss}(x, t) = \sqrt{u_{l,init}^2 + 2gx} \quad (8)$$

and

$$\alpha_{g,ss}(x, t) = 1 - \frac{(1 - \alpha_{g,init})u_{l,init}}{\sqrt{u_{l,init}^2 + 2gx}} \quad (9)$$

in which, the subscript 'ss' denotes the steady-state condition.

Table I. Parameters, initial and boundary conditions for the water faucet problem

Parameter	Value	Unit
Pipe length (L)	12	[m]
Gravity (g)	9.81	[m/s ²]
$u_{l,init}$	10	[m/s]
$u_{g,init}$	0	[m/s]
$\alpha_{g,init}$	0.2	[-]
p_{init}	10^5	[Pa]
$u_{l,inlet}$	= $u_{l,init}$	[m/s]
$u_{g,inlet}$	= $u_{g,init}$	[m/s]
$\alpha_{g,inlet}$	= $\alpha_{g,init}$	[-]
p_{outlet}	10^5	[Pa]

2.3. High-resolution Spatial Discretization Scheme

We have adapted a high-resolution spatial discretization scheme on staggered grid mesh in our previous work [15] for single- and two-phase flow thermal-hydraulics problems. The high-resolution scheme was obtained by introducing the linear reconstruction of the variable solutions and slope limiter into the original first-order upwind method (see the original discussion in [16]). For the purpose of completeness, the spatial discretization scheme is briefly discussed in this subsection.

For the staggered grid mesh commonly used in existing reactor safety system codes, scalar variables (such as pressure and density) are arranged in cell centers, while vector variables (such as velocity) are arranged on cell edges.

One major difference between the high-resolution scheme and the first-order scheme is the way with which the advection terms are treated. Though, in both schemes, the discretization of the advection terms uses the same concept of donor cells, the donor values used are different for these two schemes. In the first-order spatial discretization scheme, the advection terms in the mass equations are discretized as,

$$\left. \frac{\partial(\alpha_g \rho_g u_g)}{\partial x} \right|_i = \frac{1}{\Delta x} [(\alpha_g \rho_g u_g)_{i+1/2}^* - (\alpha_g \rho_g u_g)_{i-1/2}^*] \quad (10)$$

and

$$(\alpha_g \rho_g u_g)_{i+1/2}^* = u_{g,i+1/2} \begin{cases} \alpha_{g,i} \rho_{g,i} & \text{if } u_{g,i+1/2} > 0 \\ \alpha_{g,i+1} \rho_{g,i+1} & \text{otherwise} \end{cases} \quad (11)$$

The discretization of the advection term in the momentum equations is,

$$u_g \frac{\partial u_g}{\partial x} \Big|_{i+1/2} = \frac{1}{\Delta x} u_{g,i+1/2} \begin{cases} u_{g,i+1/2} - u_{g,i-\frac{1}{2}} & \text{if } u_{g,i+1/2} > 0 \\ u_{g,i+3/2} - u_{g,i+\frac{1}{2}} & \text{otherwise} \end{cases} \quad (12)$$

The high-resolution version of the discretization is obtained by replacing the donor values with linearly reconstructed cell edge values. Equations (11) and (12) become,

$$(\alpha_g \rho_g u_g)_{i+1/2}^* = u_{g,i+1/2} \begin{cases} \alpha_{g,i+1/2}^- \rho_{g,i+1/2}^- & \text{if } u_{g,i+1/2} > 0 \\ \alpha_{g,i+1/2}^+ \rho_{g,i+1/2}^+ & \text{otherwise} \end{cases} \quad (13)$$

and

$$u_g \frac{\partial u_g}{\partial x} \Big|_{i+1/2} = \frac{1}{\Delta x} u_{g,i+1/2} \begin{cases} u_{i+1}^- - u_i^- & \text{if } u_{g,i+1/2} > 0 \\ u_{i+1}^+ - u_i^+ & \text{otherwise} \end{cases} \quad (14)$$

in which, the superscript ‘+’ and ‘-’ denote reconstructed values (**Figure 2**). The reconstructions of variables are done using the slope limiter concept. For example, the reconstruction of scalar variable in the i^{th} volume can be done as,

$$\psi_{i+1/2}^- = \psi_i + \frac{\Delta x}{2} \psi_{x,i} \quad (15)$$

in which, $\psi_{x,i}$ is the reconstructed slope, which can be obtained by any standard slope limiter schemes, such as the Van Albada slope limiter used in this work. For more details on the high-resolution spatial discretization scheme, readers are referred to the original work by Stelling and Duinmeijer [16].

3. NEW ANALYTICAL SOLUTIONS AND NUMERICAL VERIFICATION

In this section, the derivation of an extension of Ransom’s solutions for the transient conditions (assuming separate liquid and gas pressures) and a new set of analytical solutions for the steady state conditions (assuming single pressure) will be presented. The extension of Ransom’s solutions follows the original Ransom’s assumptions and the solutions are extended to include a transient distribution of the gas phase velocity and pressure. The new analytical solutions for the steady state conditions assume a single pressure, and are the exact solutions to the two-phase equations, which can be used for the purpose of mesh convergence studies.

3.1. Extension to Ransom’s Solutions

The derivation of the gas phase velocity and pressure distribution follows Ransom’s original assumptions. Therefore, the derivation directly starts from the two-phase equations (Equations (1)-(4)) and Ransom’s solutions (Equations (6) and (7)). Following Ransom’s assumptions, the liquid phase admits a ‘free fall’ motion, and the pressure gradient in the liquid phase is ignored (a uniform pressure distribution). We also assume that the pressures for liquid phase and gas phase can be different. Here, we further assume that: the gas phase is also nearly incompressible.

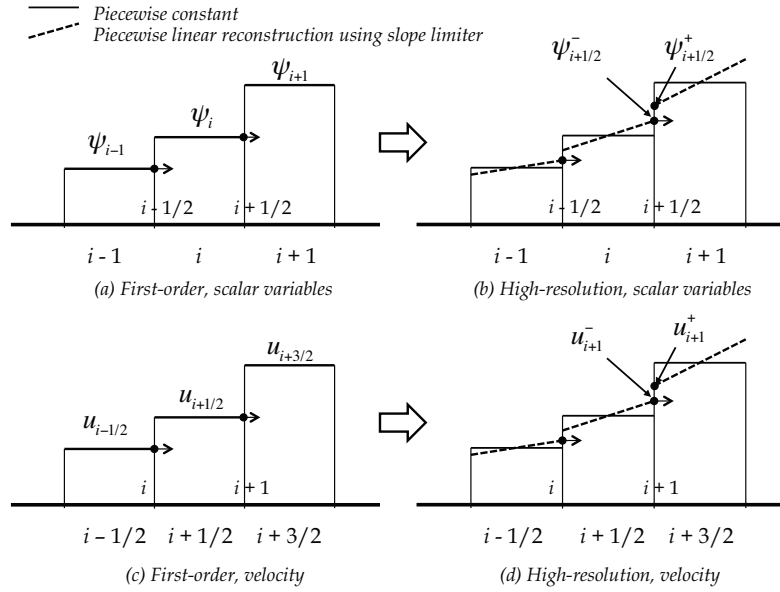


Figure 2. Schematic illustration of the first-order and high-resolution spatial discretization schemes for the staggered grid mesh. Positive velocities are assumed in this plot. ψ represents scalar properties (such as pressure and density), and u is velocity.

The gas phase velocity can be obtained by integrating the gas phase mass equation, from 0 to x ,

$$\int_0^x \left[\frac{\partial(\alpha_g \rho_g)}{\partial t} + \frac{\partial(\alpha_g \rho_g u_g)}{\partial x} \right] dx = 0 \quad (16)$$

With the subsequent manipulations: 1) applying Leibniz's rule on the first term on the left hand side; 2) applying gas phase velocity boundary condition $u_g(0, t) = 0$; and 3) assuming ρ_g is constant (nearly incompressible); the following is obtained,

$$\frac{d}{dt} \left[\int_0^x \alpha_g(x, t) dx \right] + \alpha_g(x, t) u_g(x, t) = 0 \quad (17)$$

By substituting the known void fraction distribution (Equation (7)) into Equation (17), the gas phase velocity is obtained as,

$$u_g(x, t) = \begin{cases} 0 & \text{if } x \leq u_{l,init} t + gt^2/2 \\ -\frac{1 - \alpha_{g,init}}{\alpha_{g,init}} gt & \text{otherwise} \end{cases} \quad (18)$$

The transient solution for the gas pressure can be obtained by substituting Equation (18) into the gas phase momentum equation (Equation (4)), and then integrating from 0 to x . However, due to the discontinuity in the gas phase velocity, the integration needs to be carried out in three parts to obtain the entire pressure distribution in the pipe. The first part of the integration covers the region beyond the discontinuity point. Integrating from a position beyond the discontinuity point ($x > u_{l,init} t + gt^2/2$) to L ,

$$\int_x^L \left[\frac{\partial u_g}{\partial t} + u_g \frac{\partial u_g}{\partial x} + \frac{1}{\rho_g} \frac{\partial p}{\partial x} - g \right] dx = 0 \quad (19)$$

yields the following pressure distribution,

$$p_g(x, t) = p_{outlet} - \frac{\rho_g g (L - x)}{\alpha_{g,init}} \quad \text{for } x > u_{l,init} + gt^2/2 \quad (20)$$

The second part of the integration covers the narrow region across the discontinuity point at $x_d = u_{l,init} + gt^2/2$ where the pressure jump occurs. The pressure jump can be obtained by integrating the gas phase momentum equation near the discontinuity, as shown in **Figure 3**,

$$\lim_{\substack{x_2 \rightarrow x_d^+ \\ x_1 \rightarrow x_d^-}} \int_{x_1}^{x_2} \left[\frac{\partial u_g}{\partial t} + u_g \frac{\partial u_g}{\partial x} + \frac{1}{\rho_g} \frac{\partial p}{\partial x} - g \right] dx = 0 \quad (21)$$

Note that, by taking the limit, $x_2 \rightarrow x_d^+$ and $x_1 \rightarrow x_d^-$, both the first and the fourth terms in the integral become zero, and the remaining two terms yield the following pressure jump,

$$p_1 - p_2 = \frac{1}{2} \rho_g (u_{g,2}^2 - u_{g,1}^2) = \frac{1}{2} \rho_g \left(\frac{1 - \alpha_{g,init}}{\alpha_{g,init}} gt \right)^2 \quad (22)$$

Equation (22) can also be obtained by applying the Bernoulli's equation across the discontinuity.

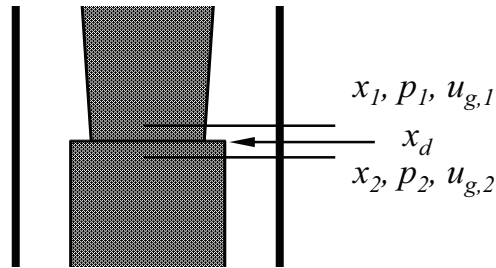


Figure 3. Integration near the discontinuity, $x_d = u_{l,init} + gt^2/2$.

The third part of the integration covers the region between the pipe inlet (top) and the discontinuity point. The pressure in this region, e.g. from 0 to ($x < u_{l,init}t + gt^2/2$), can be obtained the same way by integrating the gas phase momentum equation from 0 to x . The resulting solution for the pressure distribution can be summarized as,

$$p_g(x, t) = \begin{cases} p_{outlet} - \frac{\rho_g g (L - x_d)}{\alpha_{g,init}} + \frac{1}{2} \rho_g \left(\frac{1 - \alpha_{g,init}}{\alpha_{g,init}} gt \right)^2 - \rho_g g (x_d - x) & \text{if } x \leq u_{l,init} + gt^2/2 \\ p_{outlet} - \frac{\rho_g g (L - x)}{\alpha_{g,init}} & \text{otherwise} \end{cases} \quad (23)$$

in which, x_d is the location of the discontinuity. At steady state, the discontinuity does not exist and the pressure distribution becomes,

$$p_g(x, t) = p_{outlet} - \rho_g g (L - x) \quad (24)$$

Numerical simulations of Equations (1)~(4) were performed using two different options: 1) first-order method (first-order spatial discretization scheme and first-order Backward Euler time integration scheme), and 2) high-order method (high-resolution spatial discretization scheme and second-order Crank-Nicolson time integration scheme). Simulation results were obtained at different times, 0.3s, 0.4s, and 0.5s, using 96 cells and a time step at $10^{-3}s$. Simulation results are plotted in **Figure 4 - Figure 7** along with the new analytical solutions derived in this subsection. With the exception of the gas pressure, the numerical results for all other variables (void fraction and velocities of both phases) agree with the analytical solutions very well. It can also be found that the high-order method gives better numerical results in terms of capturing the spatial discontinuities in solutions. The simulation results of the pressure (from the single pressure equation set), however, differ significantly from the analytical gas pressure and analytical liquid pressure. The numerical results from the first-order method are able to capture the location of discontinuity (though smeared a lot), the pressure distribution between the location of discontinuity and pipe exit, and the slope of the pressure distribution between the pipe inlet and the location of discontinuity. Overall, the transient trend of the pressure distribution agrees with analytical solutions. However, the pressure jump across the discontinuity is largely over-predicted. The numerical results from the high-order method shows a different trend compared to the first-order method. Though it captures the location of discontinuity (less smeared), the transient trend of pressure distribution does not follow the analytical solutions. Such an unstable behavior was also observed in the work [12] (see results presented in sections 3.4, 4.2 and 6.4 of reference [12]). There is no clear answer for such behaviors. There are several possibilities that the numerical results do not agree well with the analytical solution for the pressure. First, some of the assumptions made, for example the incompressible flow assumption for both phases, are inadequate for the derivation of the solutions for pressure. Second, the derivation of the analytical solutions assumes that pressures are different between the two phases. The numerical results, however, are obtained from the equation set constrained by the single pressure assumption. The inconsistency between how the analytical solutions and numerical solutions are obtained could cause the disagreement between them. The disagreement also reminds us that the Ransom's solutions and our extension based on them are only approximated analytical solutions. Also, it has to be pointed out that the Ransom's solutions (and our extensions) cannot be used for strict mesh convergence study due to the two pressure assumptions made. In order to do mesh convergence study, analytical solutions based on single-pressure conditions have to be derived. This will be demonstrated in the next subsection. However, only solutions at the steady state can be obtained.

3.2. Analytical Solutions at Steady State with Single Pressure

The derivation of the analytical solutions at the steady state is relatively simple. However, to the authors' best knowledge, it is not available in literatures. The derivation simply starts from the steady-state gas phase mass equation (Equation (2) without transient term). By integrating from 0 to x , and applying gas phase velocity boundary condition, $u_g(x = 0) = 0$, it can be obtained that,

$$u_{g,ss}(x) = 0 \quad (25)$$

in which, subscript 'ss' denotes the steady-state condition. By substituting Equation (25) into the steady-state gas phase momentum equation (Equation (4) without transient term), it can be obtained that:

$$\frac{1}{\rho_g} \frac{dp}{dx} - g = 0 \quad (26)$$

If the gas phase density, ρ_g , is an integrable function of pressure, p , which is true for most equations of state, Equation (26) can be integrated to get the pressure function, $p(x)$. For the purpose of demonstration,

the linearized equation of state is used and incompressible approximation was adapted for both the liquid and the gas phase, which only introduces trivial errors. Thus, the pressure distribution can be obtained as,

$$p_{ss}(x) = p_{outlet} - \rho_g g(L - x) \quad (27)$$

The liquid phase velocity at the steady state can be obtained by substituting Equation (27) into the steady-state liquid phase momentum equation,

$$u_{l,ss}(x) = \sqrt{u_{l,init}^2 + 2g_{eff}x} \quad (28)$$

in which, g_{eff} is the effective gravity considering the effect of gas phase pressure on the liquid phase. It is defined as,

$$g_{eff} = g \left(1 - \frac{\rho_g}{\rho_l}\right) \quad (29)$$

The void fraction distribution at the steady state can be obtained from the liquid phase mass equation:

$$\alpha_{g,ss}(x) = 1 - \frac{(1 - \alpha_{g,inlet})u_{l,inlet}}{u_{l,ss}(x)} \quad (30)$$

Comparing this set of analytical solutions (Equations (28) and (30)) with Ransom's solutions (Equations (8) and (9)), it can be found that the only difference is: in our analytical solutions the effective gravity replaces the gravity in Ransom's solutions. In other words, the massless gas phase assumption used in Ransom's derivation is removed in this work. Also, it is noted that, the new solution, equations (28) and (30) exactly reduces to equations (8) and (9), if the massless gas phase assumption could be made. Using the high-resolution spatial discretization scheme (second-order accuracy with spatially smooth solutions) described in section 2.3, and a second-order Crank-Nicolson implicit time integration scheme, mesh refinement study was performed for different numbers of cells, ranging from 12 to 192. Both the Ransom's analytical solutions (Equations (8) and (9)) and the new analytical solutions derived in this subsection were used as the reference solutions. The results of the mesh convergence studies are summarized in **Table II** using Ransom's solutions, and **Table III** using our solutions, respectively. It is clear that a second-order of spatial accuracy is obtained by using the analytical solutions derived in this work, which considers the effect of pressure distribution in the gas phase (i.e., single pressure condition). On the contrary, the Ransom's solutions are not able to give a second-order of spatial accuracy due to the simplifications made. The numerical simulation results are also plotted against our new analytical solutions in **Figure 8** and **Figure 9**, using 48 cells. The numerical results overlap with the analytical solutions very well.

Table II. Spatial convergence rate, using the Ransom's solutions as the reference

N_{cell}	$\Delta x=L/ N_{cell}$	α_g		u_l	
		L-1 Norm	Convergence Rate	L-1 Norm	Convergence Rate
12	1	1.9884E-02	-	2.7079E-01	-
24	0.5	6.1237E-03	1.70	8.9284E-02	1.60
48	0.25	2.1802E-03	1.49	3.9990E-02	1.16
96	0.125	1.1253E-03	0.95	2.7052E-02	0.56
192	0.0625	8.5615E-04	0.39	2.3701E-02	0.19

4. DISCUSSIONS AND CONCLUSIONS

In this work, we have derived analytical solutions to extend the Ransom's solutions under transient conditions for the water faucet problem, which follows Ransom's original assumptions. Numerical results from transient simulations agreed with these analytical solutions very well, with the exception of the pressure distribution. This might be due to the inconsistency between two different pressures used for the two phases to derive the analytical solutions and the single-pressure constraint from the equation set used to obtain the numerical results. The causes for the unstable pressure distribution warrant further investigation in the future work.

Strictly following the single-pressure condition of the two-phase flow equations, we have also derived a new set of analytical solutions for the water faucet problem at the steady-state condition. The derived steady-state analytical solutions were used for mesh convergence study of the high-resolution spatial discretization scheme, from which the expected second-order of accuracy was achieved.

ACKNOWLEDGMENTS

This work is supported by the U.S. Department of Energy, under Department of Energy Idaho Operations Office Contract DE-AC07-05ID14517. Accordingly, the U.S. Government retains a nonexclusive, royalty-free license to publish or reproduce the published form of this contribution, or allow others to do so, for U.S. Government purposes.

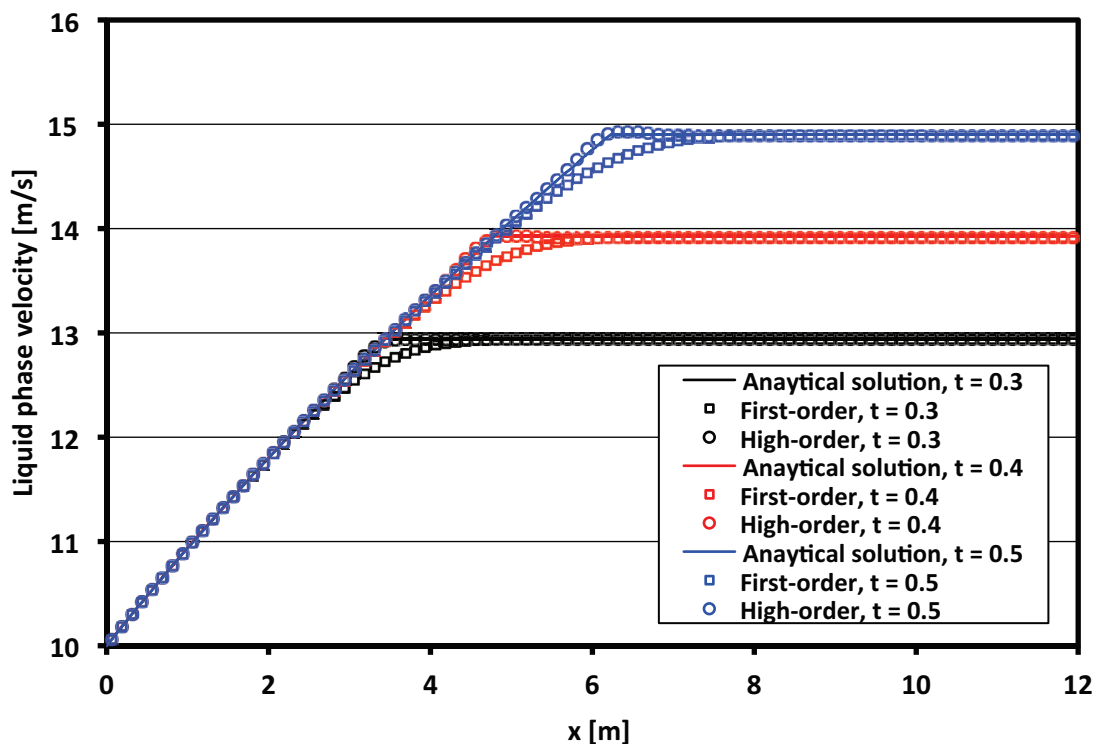


Figure 4. Numerical results of liquid phase velocity with analytical solutions at 0.3, 0.4 and 0.5s.

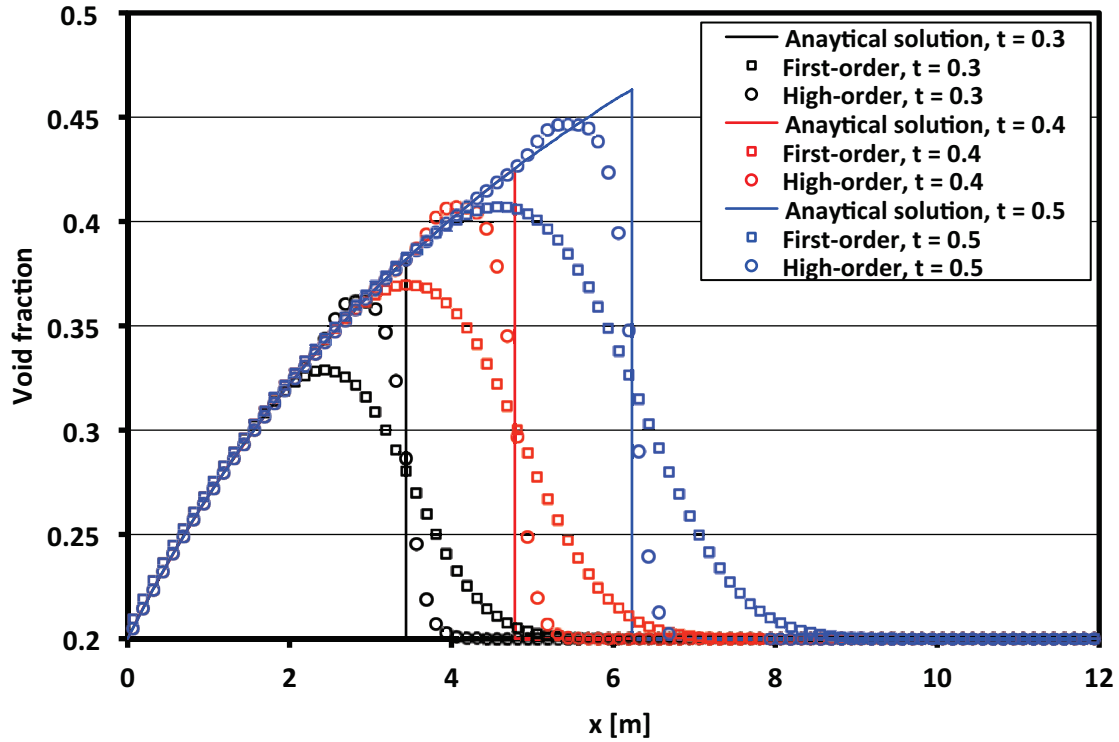


Figure 5. Numerical results of void fraction with analytical solutions at 0.3, 0.4 and 0.5s.

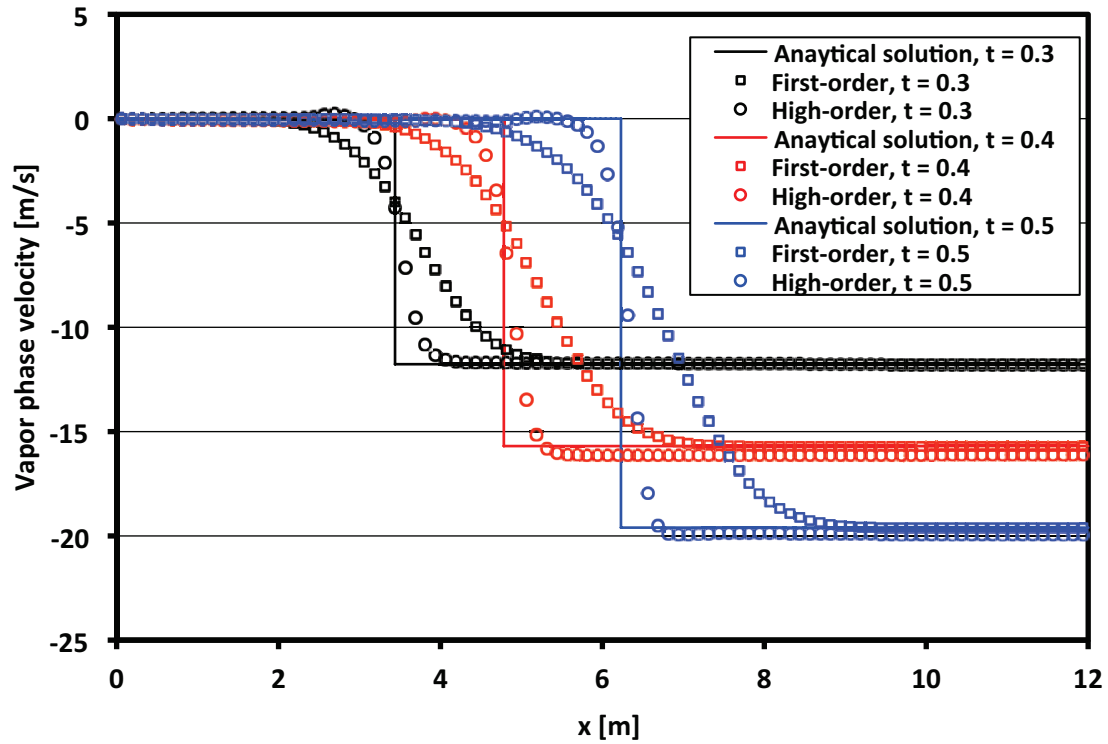


Figure 6. Numerical results of gas phase velocity with analytical solutions at 0.3, 0.4 and 0.5s.

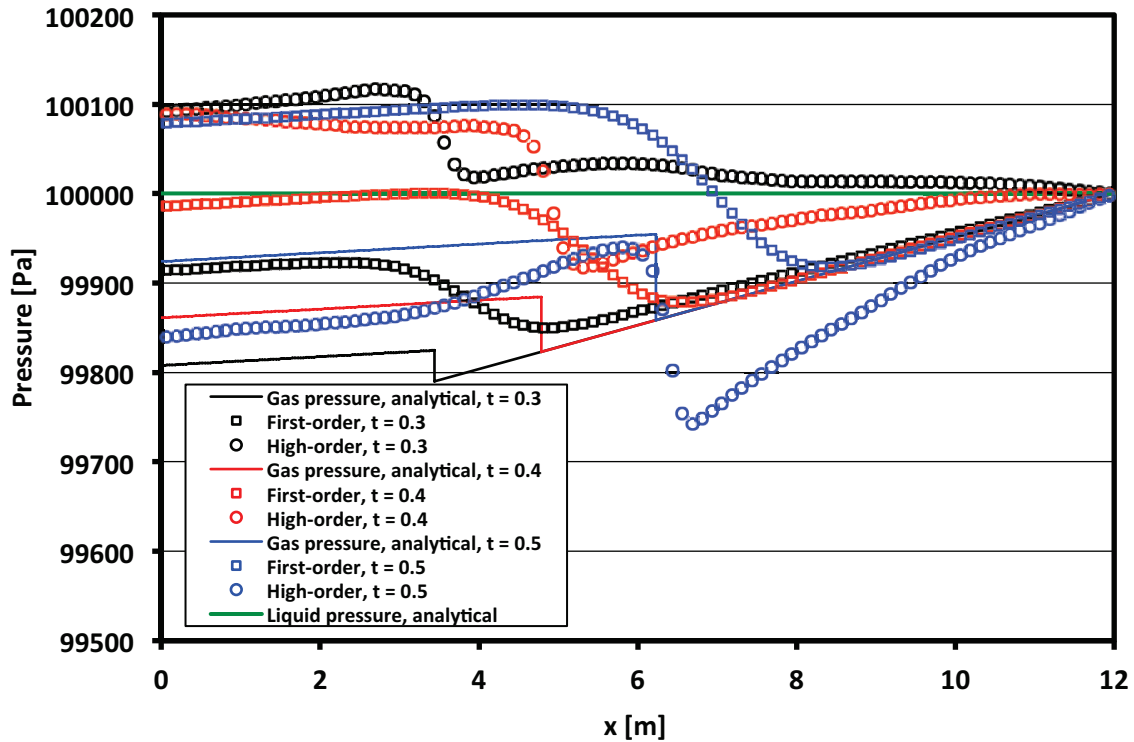


Figure 7. Numerical results of pressure with analytical solutions at 0.3, 0.4 and 0.5s.

Table III. Spatial convergence rate, using the new analytical solutions derived in subsection 3.2 as the reference

N_{cell}	$\Delta x=L/ N_{cell}$	α_g		u_l	
		L-1 Norm	Convergence Rate	L-1 Norm	Convergence Rate
12	1	1.9267E-02	-	2.4671E-01	-
24	0.5	5.4304E-03	1.83	6.5983E-02	1.90
48	0.25	1.4487E-03	1.91	1.7085E-02	1.95
96	0.125	3.7463E-04	1.95	4.3471E-03	1.97
192	0.0625	9.5424E-05	1.97	1.0953E-03	1.99

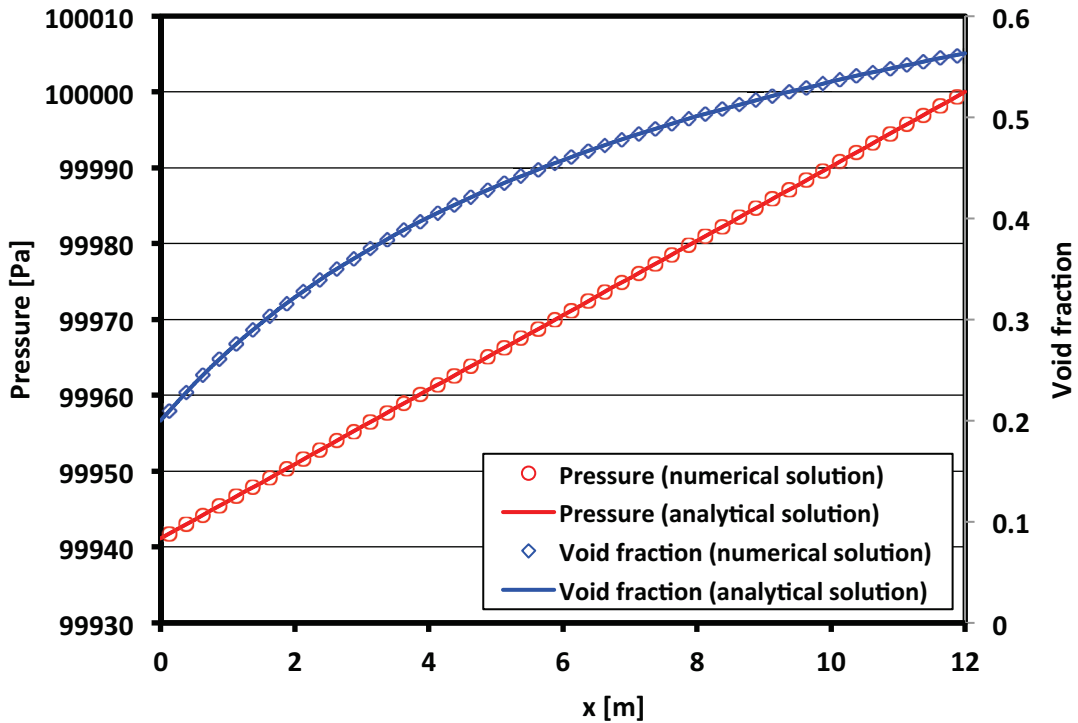


Figure 8. Numerical results of pressure and void fraction with analytical solutions at the steady state.

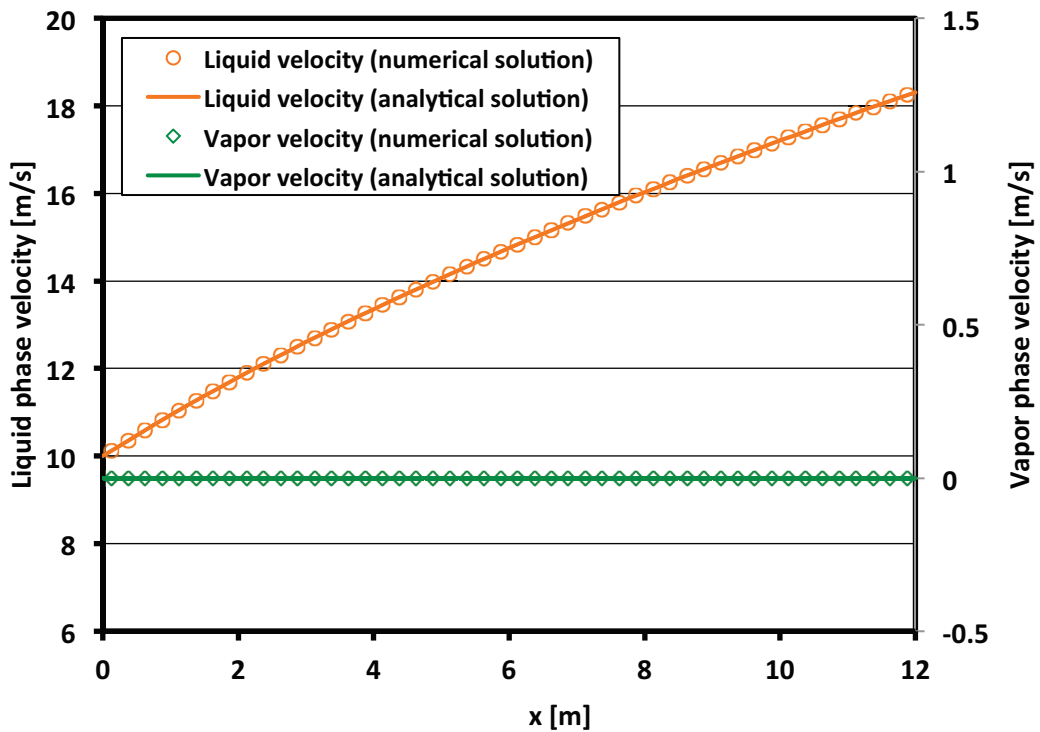


Figure 9. Numerical results of liquid and gas phase velocities with analytical solutions at the steady state.

REFERENCES

1. Numerical Benchmark Test, volume 2 of Multiphase Science and Technology, Edited by G.F. Hewitt, J.M. Delhay, and N. Zuber, John Wiley & Sons Ltd., 1987.
2. "RELAP5-3D Code Manual Volume III: Developmental Assessment", INEEL-EXT-98-00834, Revision 4.0, September 2012.
3. H. Lim et al., "Application of Hyperbolic Two-fluids Equations to Reactor Safety Code", *Journal of the Korean Nuclear Society*, **Vol. 35, No. 1**, pp. 45-54 (2003).
4. R. A. Abu Saleem and T. Kozlowski, "Development of Accurate and Stable Two-Phase Two-Fluid Model Solver", *Proceedings of ICAPP 2014*, Charlotte, USA, April 6-9 (2014).
5. F. Coquel et al., "A Numerical Method Using Upwind Schemes for the Resolution of Two-Phase Flows", *J. Comp. Phys.*, **136**, 272-288 (1997).
6. J. R. García-Cascales, "Conservative numerical schemes for unsteady 1D two-phase flow", PhD thesis, Universidad Politécnica de Valencia, Spain (2001).
7. F. Benkhaldoun and L. Quivy, "A non homogeneous Riemann Solver for shallow water and two phase flows", *Flow Turbulence Combustion*, **Vol. 76**, pp.391-402 (2006).
8. M.F. Jerez-Carrizales et al., "Simulation of the two phase flow in a wellbore using two-fluid model", *11th World Congress on Computational Mechanics*, Barcelona, Spain, 20-25 July, (2014).
9. S.T. Munkejord, "Partially-reflecting boundary conditions for transient two-phase flow", *Commun. Numer. Meth. Engng*, **22**, pp. 781-795 (2006).
10. T. Gallouet et al., "Numerical modeling of two-phase flows using the two-fluid two-pressure approach", *Mathematical Models and Methods in Applied Sciences*, **Vol. 14, No. 15**, pp.663-700 (2004).
11. P. Loilier and C. Omgba-Essama, "Numerical experiments of two-phase flow in pipelines with a two-fluid compressible model", 12th International Conference on Multiphase Production Technology, Barcelona, Spain, May 25-27 (2005)
12. S.T. Munkejord, "Analysis of the two-fluid model and the drift-flux model for numerical calculation of two-phase flow", PhD thesis, Norwegian University of Science and Technology (2006).
13. W.D. Fullmer et al., "An Artificial Viscosity for the Ill-Posed One-Dimensional Incompressible Two-Fluid Model", *Nuclear Technology*, **Vol. 185, No. 3**, pp. 296-308 (2014).
14. R. J. LeVeque, *Finite-Volume Methods for Hyperbolic Problems*, Cambridge University Press (2004)
15. L. Zou, H. Zhao and H. Zhang, "Applications of high-resolution spatial discretization scheme and Jacobian-free Newton-Krylov method in two-phase flow problems," *Annals of Nuclear Energy*, **Vol. 83**, pp. 101-107, (2015).
16. G.S. Stelling and S.P.A. Duinmeijer, "A staggered conservative scheme for every Froude number in rapidly varied shallow water flows", *Int. J. Numer. Meth. Fluids*, **Vol. 43**, pp. 1329-1354 (2003).
17. "RELAP5/MOD3.3 Code Manual Volume I", NUREG/CR- 5535 ed., U.S. Nuclear Regulatory Commission, December, 2001.
18. "TRAC-M/FORTRAN 90 (Version 3.0) Theory Manual", NUREG/CR-6724 ed., U.S. Nuclear Regulatory Commission, April, 2001.
19. "TRACE V5.0 Theory Manual", Division of Risk Assessment and Special Projects Office of Nuclear Regulatory Research, U. S. Nuclear Regulatory Commission Washington, DC 20555-0001.
20. V.H. Ransom, "Faucet Flow, Oscillating Manometer, and Expulsion of Steam by Subcooled Water," *Part III, Numerical Benchmark Tests, Multiphase Science Technology*, Volume 3 (1979).
21. "RELAP5/MOD3 Code Manual, Volume 6: Validation of Numerical Techniques in RELAP5/MOD3", NUREG/CR-5535, EGG-2596, October (1994).